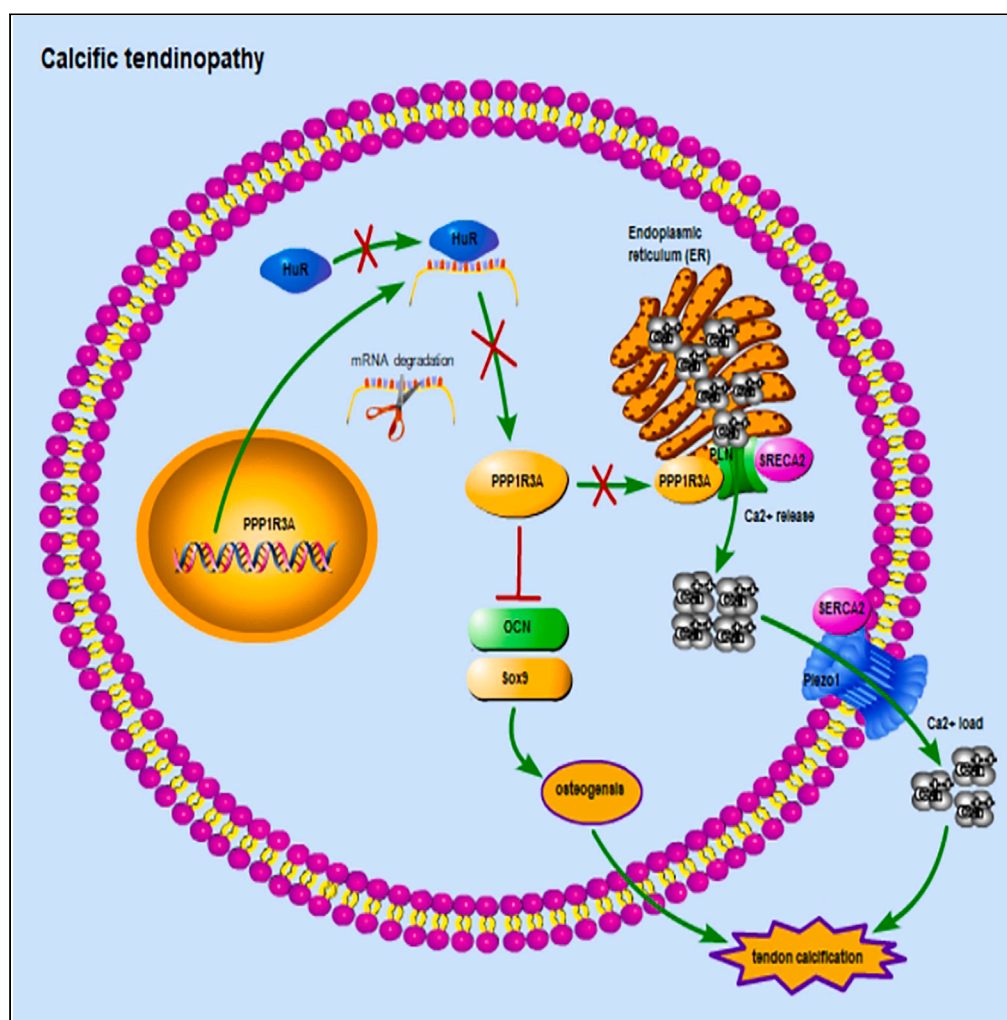


Article

PPP1R3A inhibits osteogenesis and negatively regulates intracellular calcium levels in calcific tendinopathy



Chao Hu, Lin Ma,
Shang Gao, ...,
Bing-Hua Zhou,
Wan Chen, Kang-
Lai Tang

chenwanfred@foxmail.com
(W.C.)
tangkanglai@hotmail.com
(K.-L.T.)

Highlights

Identification of PPP1R3A
as a protector in calcific
tendinopathy (CT)

Pathological effects of CT
in rat can be reversed by
overexpression of
PPP1R3A

PPP1R3A expression was
regulated at the
posttranscriptional level by
binding of HuR

PPP1R3A regulates calcium
homeostasis in tendon
cells via Piezo1/SERCA2s

Article

PPP1R3A inhibits osteogenesis and negatively regulates intracellular calcium levels in calcific tendinopathy

Chao Hu,^{1,2} Lin Ma,¹ Shang Gao,¹ Ming-Yu Yang,¹ Mi-Duo Mu,¹ Le Chang,¹ Pan Huang,¹ Xiao Ye,¹ Wei Wang,¹ Xu Tao,¹ Bing-Hua Zhou,¹ Wan Chen,^{1,*} and Kang-Lai Tang^{1,3,*}

SUMMARY

Calcific tendinopathy (CT) is defined by the progressive accumulation of calcium crystals in tendonic regions that results in severe pain in patients. The etiology of CT is not fully elucidated. In this study, we elucidate the role of PPP1R3A in CT. A significant decrease in PPP1R3A expression was observed in CT patient tissues, which was further confirmed in tissues from a CT-induced rat model. Overexpression of PPP1R3A *ex vivo* reduced the expression of osteo/chondrogenic markers OCN and Sox9, improved tendon tissue architecture, and reduced intracellular Ca²⁺ levels. Overexpression of SERCA2 and knock-down of Piezo1 decreased expression of osteo/chondrogenic markers and intracellular calcium in PPP1R3A-knockdown tendon cells. Lastly, PPP1R3A expression was regulated at the posttranscriptional level by binding of HuR. Collectively, the present study indicates that PPP1R3A plays an important role in regulating calcium homeostasis in tendon cells via Piezo1/SERCA2, rendering it a promising target for therapeutic interventions of CT.

INTRODUCTION

Calcific tendinopathy (CT) is a result of cumulative deposition of calcium in the rotator cuffs of the tendons that is often resorbed slowly due to several unknown parameters. Approximately 10% of the adult population develops CT during mid- or later stages of life and women are more predisposed to CT when compared to men.^{1,2} Unresolved calcifications in the joints result in symptoms such as acute pain and uneasiness in patients. Conventional treatment includes systemic treatment options such as anti-inflammatory drugs and corticosteroids and in most cases also physical therapy.³ The formative phase of CT involves the formation and accumulation of calcium crystals. This phase is either non-symptomatic or patients present with low-grade pain. However, the resorptive phase is acute and patients experience severe pain with localized swelling.^{4,5}

The etiology of CT is still largely unknown. Several pathological processes such as tenocyte necrosis and endochondral ossification have been described to contribute to the development of CT, along with other factors such as age and body mass index.^{6–8} Tendon cells are important for homeostatic maintenance in the healthy tendon and to promote tissue healing after injury. The fate of tendon cells is dictated by their local microenvironment and extracellular matrix (ECM) organization and composition.^{9,10} Nontenocyte differentiation into osteoblasts or chondrocytes in response to external cues such as injuries or mechanical stress may also result in tendinopathy.^{11–13} Therefore, dysfunction of cell-mediated processes is a major contributor to the pathogenesis of CT. While matrix-associated changes have been studied before,¹⁴ defective cellular processes that contribute toward calcification and tendinopathy have been poorly understood so far. In contrast to systemic drugs, Famotidine, which specifically blocks the histamine receptor-2, has been shown to suppress calcification in tendon tissues.¹⁵

Protein phosphatase 1 regulatory subunit 3A (PPP1R3A) is a regulator of serine/threonine protein phosphatases that enhances dephosphorylation of glycogen substrates and regulates membrane channels and receptors.¹⁶ Notably, recent research has shown that PPP1R3A is a RyR2-binding partner and demonstrates that loss of PPP1R3A promotes abnormal calcium (Ca²⁺) release from the sarcoplasmic reticulum (SR) and increases atrial fibrillation susceptibility in mice.¹⁷ Disruption of Ca²⁺ homeostasis leads to the disorder of many different cellular functions such as metabolism, cell proliferation, division and differentiation, programmed cell death, and muscle excitation-contraction. One study reported that the difference in the osteogenic differentiation of the tendon stem/progenitor cells (TSPCs) is related to the ion concentrations of the TSPCs medium (Ca²⁺ and inorganic phosphate ion).¹⁸ Increased Ca²⁺ signaling induces tendon collagen fibrillogenesis during tendon hypertrophy.¹⁹ But knowledge about Ca²⁺ signaling and the source of Ca²⁺ signals in tendon cell biology and the pathogenesis of CT is largely unknown. By comparing gene expression data from tendinopathy patients and healthy adults from a previously described

¹Department of Sports Medicine Center, Southwest Hospital, Army Medical University, Chongqing 400000, China

²Department of Orthopedics, 904 Hospital of PLA, Wuxi 214000 Jiangsu, China

³Lead contact

*Correspondence: chenwanfred@foxmail.com (W.C.), [tangkanlai@hotmail.com](mailto:tangkanglai@hotmail.com) (K.-L.T.)

<https://doi.org/10.1016/j.isci.2023.107784>



study,²⁰ we identified that PPP1R3A was downregulated in tendinopathy. We presume that loss of PPP1R3A may affect the tendon cell functions via disrupting Ca²⁺ homeostasis. However, the function and mechanism of PPP1R3A in the pathogenesis of CT remains a mystery.

As the largest intracellular Ca²⁺ reservoir, the sarco/endoplasmic reticulum (SR/ER) plays a key role in the regulation of Ca²⁺ homeostasis.²¹ Interruption of Ca²⁺ homeostasis in the ER leads to activation of ER stress-coping responses, for instance, the unfolded protein response (UPR).²² The accumulated evidence suggests that constant interrupting Ca²⁺ homeostasis and chronic ER stress could lead to kidney disease,²³ neurodegenerative disorders,²⁴ or cancer.²⁵ PPP1R3A mediates PP1c regulation of both RyR2 and PLN within an extended RyR2/PLN/SERCA2a complex that as joint Ca²⁺ release/re-uptake regulatome complexes.¹⁷ SERCA2 is indispensable for the maintenance of calcium homeostasis via pumping Ca²⁺ back to the SR/ER, especially in cardiomyocytes and neuronal cells.^{26,27} Moreover, Piezo proteins 1 and 2 act as mechanosensitive membrane channels in various cell types. Piezo1 selectively conducts cations, for instance, Na⁺, K⁺, Ca²⁺, and Mg²⁺, with a slight preference for Ca²⁺.^{28,29} Specifically, Piezo1 acts as a high-strain mechanosensory channel in chondrocytes.^{30,31} It has two distinct functions: a mechanotransduction module and a central pore region. The activity between these two functions is regulated by sarco-plasmic/endoplasmic-reticulum Ca²⁺ ATPase 2 (SERCA2) by interaction with Piezo1.³² Additionally, accumulating evidence suggested that Piezo1 plays a major role in stem cell fate determination in multiple differentiation processes.³³

In this study, we describe an underlying mechanism underlying the regulation of intracellular calcium levels in tendon cells by PPP1R3A through Piezo1 and SERCA2 under pathological conditions using an *in vivo* collagenase-based calcification rat model.

RESULTS

PPP1R3A expression is downregulated in calcific tendinopathy

To evaluate the expression of PPP1R3A in healthy individuals and tendinopathy patients, we analyzed the differently expressed genes from a previous dataset (GSE26051). Interestingly, expression of PPP1R3A in tendinopathy was lower in several tissues from tendinopathy patients when compared to healthy tendons (Figures 1A and 1B). We next performed immunohistochemistry in tendon tissues from calcified areas and normal healthy regions and observed a similar decrease in PPP1R3A expression in calcific tendons (Figures 1C and 1D). H&E staining revealed the lack of tissue architecture in calcific tendons when compared to normal tissues that showed fibroblasts with long, thin nuclei and abundant intervening collagen (Figure 1C). We also analyzed the expression of PPP1R3A by qPCR in the different tissue samples and observed a significant 4-fold decrease in mRNA expression (Figure 1E). Further, analysis of tissue lysates by SDS/PAGE, Western blot revealed a complete or partial loss of protein expression in calcific tendon tissues (Figure 1F). Together, our results show that PPP1R3A is downregulated in calcific tendinopathy.

PPP1R3A overexpression inhibits ectopic calcification and promotes tendon regeneration in a collagenase-induced rat tendon calcification model

To investigate whether PPP1R3A could be a potential therapeutic target *in vivo*, we established the rat Achilles tendon ectopic calcification model. Achilles tendon tissues from control (sham) mice and model mice, treated with PPP1R3A-overexpressing lentivirus showed an increase in PPP1R3A mRNA and protein expression when compared to control as evaluated by qPCR and Western blot, respectively (Figures 2A and 2B). Immunohistochemistry analysis in tissues from mice 12 weeks after treatment revealed the retainment of healthy tendon tissue architecture and high-PPP1R3A expression in calcific tendinopathy mice treated with PPP1R3A when compared to control (Figures 2C and 2D). Safranin O staining was generally reduced in the tendons of the PPP1R3A overexpression group when compared to control mice (Figure 2E). Consistent with the histology analyses, the expression of osteochondral differentiation-related proteins OCN and Sox9 were attenuated by PPP1R3A overexpression as observed by immunofluorescence (Figures 2F–2H). These results indicate that overexpression of PPP1R3A may prevent calcification of tendons *in vivo*.

PPP1R3A overexpression retains tissue architecture in calcific tendinopathy

To further verify the therapeutic effect of PPP1R3A overexpression histologically, we performed hematoxylin and eosin (H&E) and Masson trichrome staining. We observed that overexpression of PPP1R3A resulted in a significantly improved tissue morphology and had lower histological score compared to the control group (Figures 3A and 3B). More collagen was deposited in the tendons of the PPP1R3A-overexpression group, and the collagen fibers assembled more orderly as evidenced by Masson trichrome staining (Figure 3C). PPP1R3A overexpression also upregulated the expression of tendon related proteins COL1 and TNMD under the pathological conditions (Figures 3D–3F). Taken together, these results indicate that PPP1R3A overexpression promotes synthesis of the extracellular matrix and helps to retain healthy tissue architecture in calcific tendinopathy.

Knockdown of PPP1R3A promotes osteogenesis and increases intracellular Ca²⁺ levels

To study the role of PPP1R3A in regulating cell function, we next performed a knockdown of PPP1R3A by siRNA treatment. siRNA treatment reduced the expression of PPP1R3A in tendon cells at the mRNA and protein level (Figures 4A and 4B). CCK-8 assay revealed that knockdown of PPP1R3A reduced tendon cell proliferation; however, overexpression of PPP1R3A significantly increased cell proliferation (Figure 4C). ALP and ARS staining revealed a significant increase in alkaline phosphatase activity and ARS levels, respectively, upon PPP1R3A knockdown whereas this significantly decreased upon PPP1R3A overexpression when compared to their respective controls (Figures 4D and 4E). Furthermore, we also observed a significant increase in osteochondral differentiation-associated markers OCN and Sox9 expression in tendon cells

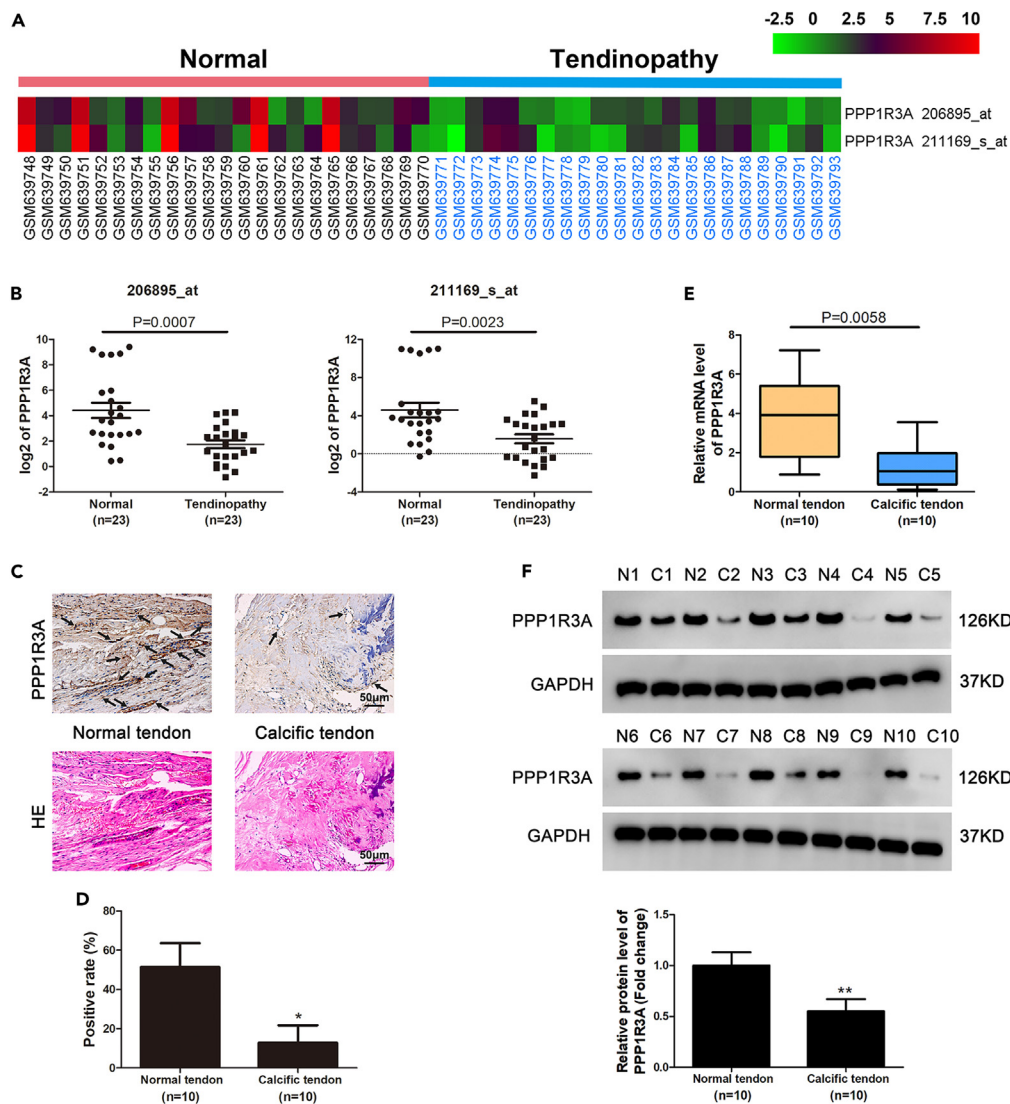


Figure 1. Expression of PPP1R3A in calcific tendinopathy

(A) Heatmap of PPP1R3A expression in tissues from healthy controls (n = 23) and tendinopathy patients (n = 23) from microarray dataset (GSE26051). Scale bar indicates high expression in red and low expression in green.

(B) Individual values from data shown in A plotted as log₂ values. p value calculated by Mann-Whitney U test.

(C) Representative immunohistochemistry images of PPP1R3A expression and H&E staining in human normal and calcific tendons. Scale bars, 50 μm.

(D) Quantification of images shown in C for total area positive for PPP1R3A expression in calcific and normal tendons (n = 10). Values are means ± SD. *p < 0.05, versus normal tendons, calculated by two-tailed paired t test.

(E) PPP1R3A mRNA levels were analyzed by qRT-PCR with GAPDH as control, n = 10. p value calculated by Mann-Whitney U test.

(F) Western blotting analysis was performed to detect the levels of PPP1R3A protein in human calcific (C) and normal tendons (N). The band intensity was normalized to GAPDH. The intensity of the blots was represented as mean ± standard deviation (SD) of ten pair tissues samples. Results are shown as the fold change of the normal tendon group on the bar graph. **p < 0.01, versus normal tendons, calculated by two-tailed paired t test.

upon knockdown of PPP1R3A (Figure 4F). We next assessed the changes in intracellular Ca²⁺ levels using the Fluo-4AM Ca²⁺ fluorescence probe and observed a significant increase in Ca²⁺ deposits upon PPP1R3A knockdown by immunofluorescence (Figure 4G). Flow cytometry analysis of calcium ion concentration also revealed a similar increase in total levels of Ca²⁺ upon knockdown of PPP1R3A (Figure 4H). Collectively, these results indicate that PPP1R3A expression directly regulates osteogenesis and intracellular Ca²⁺ levels in tendon cells.

SERCA2/Piezol regulates osteogenesis and Ca²⁺ levels in PPP1R3A-dependent manner

To identify the mechanism underlying PPP1R3A-mediated regulation of osteogenesis and Ca²⁺ levels, we assessed the role of SERCA2, a Ca²⁺-ATPase and Piezo1, a mechanosensitive ion channel. Achilles tendon tissues of control and calcification model mice were analyzed

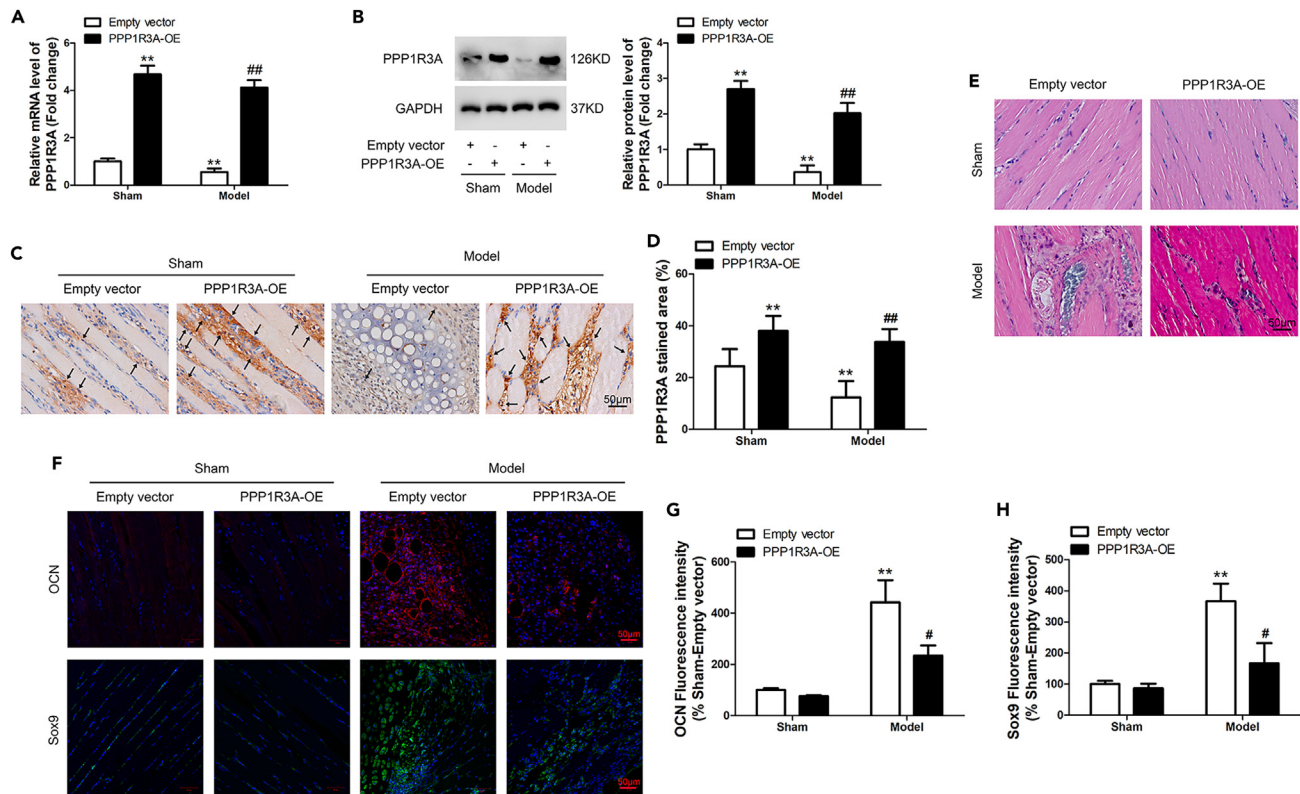


Figure 2. PPP1R3A overexpression inhibits ectopic calcification in a collagenase-induced rat tendon calcification model

(A–D) Analysis of PPP1R3A expression in rat Achilles tendon tissues from control (Sham) or tendon calcification model (Model) treated with PPP1R3A overexpressing lentivirus or empty control vector. (A) qRT-PCR analysis of PPP1R3A mRNA expression in rat Achilles tendons. (B) Western blot analysis indicating PPP1R3A protein expression in rat Achilles tendons from control (Sham) or pathological mice group (Model). The band intensity was normalized to GAPDH. (C) Representative immunohistochemistry images of PPP1R3A expression in rat Achilles tendons. Scale bars, 50 μ m. Arrows indicate the PPP1R3A + positive cells. (D) Quantification of images shown in C for total area positive for PPP1R3A expression. Values are means \pm SD (n = 6). p value calculated was determined by two-tailed unpaired Student's t test. **, ##p < 0.01. * vs. the Sham-Empty vector group, # vs. the Model-Empty vector group. (E) Representative images from Safranin O staining of Achilles tendon sections. Scale bar: 50 μ m. (F) Representative micrographs of OCN and SOX9 expression in Achilles tendon tissues visualized by immunofluorescence. Scale bar: 50 μ m. (G and H) The fluorescence intensity of OCN (G) and SOX9 (H) staining in Achilles tendon tissues. Results are shown as mean \pm SD (n = 6). p value calculated was determined by two-tailed unpaired Student's t test. *, #p < 0.05, **, ##p < 0.01. * vs. the Sham-Empty vector group, # vs. the Model-Empty vector group.

for the expression of SERCA2 and Piezo1 by Western blot and immunofluorescence. Interestingly, SERCA2 expression was decreased in control calcific model mice, which increased upon PPP1R3A overexpression (Figures 5A and 5B). On the contrary, expression of Piezo1 decreased upon PPP1R3A overexpression (Figures 5A and 5B). Similarly, knockdown of PPP1R3A reduced expression of SERCA2 and increased expression of Piezo1 in tendon cells (Figure 5C). Immunoprecipitation analysis revealed an association between SERCA2 and Piezo1 as observed by the presence of Piezo1 in anti-SERCA2 pull-down and vice versa (Figure 5D). SERCA2 overexpression also reduced the severity of PPP1R3A knockdown in osteogenesis, whereas Piezo1 knockdown also showed a similar effect (Figures 5E and 5F). SERCA2 overexpression or Piezo1 knockdown also reduced expression of OCN and Sox9, which was upregulated upon PPP1R3A knockdown (Figure 5G). Lastly, we also observed a decrease in intracellular Ca²⁺ levels upon SERCA2 overexpression or Piezo1 knockdown in tendon cells with PPP1R3A knockdown (Figure 5H). Taken together, these results reveal that PPP1R3A regulates osteogenesis and intracellular Ca²⁺ levels through SERCA2/Piezo1 in tendon cells.

HuR stabilizes PPP1R3A mRNA by binding to the 3'-UTR region

The ELAV-like RNA-binding protein 1 (ELAVL1, also called HuR) regulates stability and translation of mRNAs. To further investigate the regulation of PPP1R3A by HuR, we targeted HuR in tendon cells by siRNA treatment. Knockdown of HuR in tendon cells decreased the protein and mRNA expression levels of PPP1R3A (Figures 6A and 6B). To investigate if HuR regulates PPP1R3A expression posttranscriptionally, we next examined if HuR directly interacts with PPP1R3A mRNA in cultured tendon cells. RIP analysis using an anti-HuR antibody followed by measurement of PPP1R3A mRNA levels by qPCR revealed that PPP1R3A mRNA associates with HuR, as PPP1R3A mRNA was highly enriched

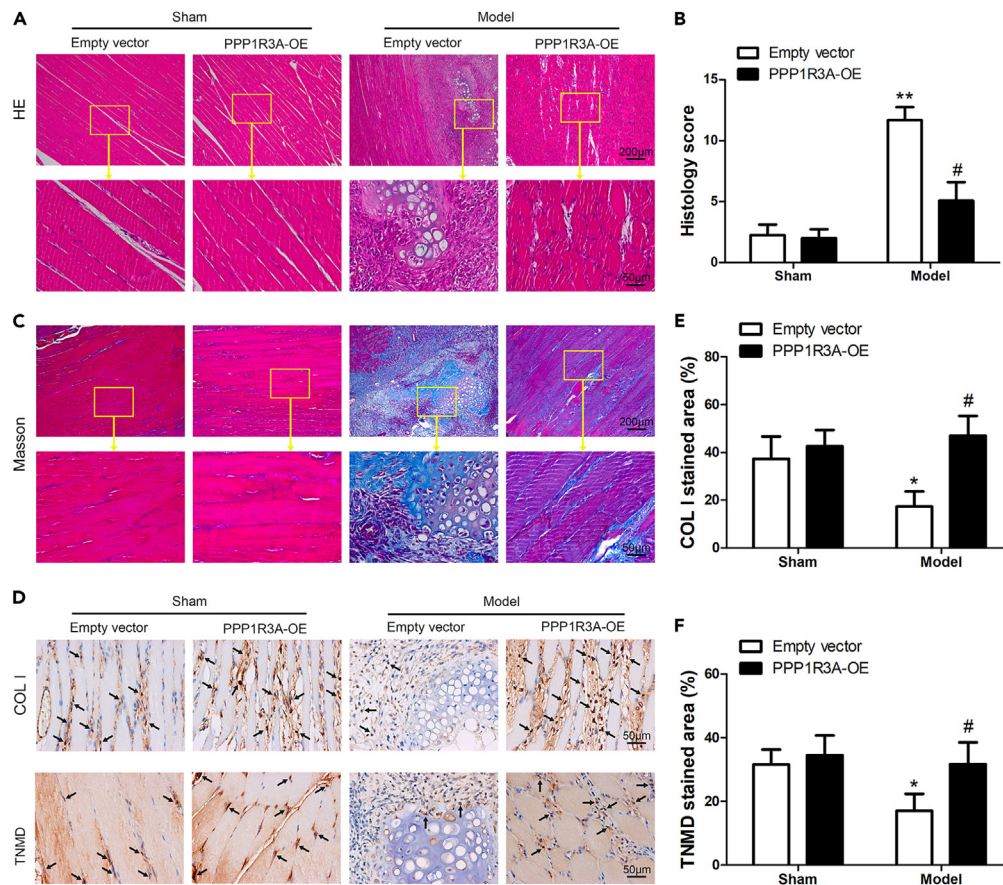


Figure 3. PPP1R3A overexpression promotes tendon regeneration in a collagenase-induced rat tendon calcification model

(A) Representative images from H&E staining in tissues from control (Sham) and calcification-induced (Model) rats.

(B) Histological score of the repaired tendon ($n = 6$). p value calculated was determined by two-tailed unpaired Student's t test. *, # $p < 0.05$, ** $p < 0.01$. * vs. the Sham-Empty vector group, # vs. the Model-Empty vector group.

(C) Masson staining of the Achilles tendon in four groups.

(D) Representative images of immunohistochemistry staining of type I collagen (COL I) and TNMD in the Achilles tendon tissue in each group. Scale bar: 50 μm . Arrows indicate the COL I+ or TNMD + positive cells.

(E and F) Quantification of images shown in D for total area positive for COL I (E) and TNMD (F) expression. Results are shown as mean \pm SD ($n = 6$). p value calculated was determined by two-tailed unpaired Student's t test. *, # $p < 0.05$. * vs. the Sham-Empty vector group, # vs. the Model-Empty vector group.

in HuR pull-down fraction relative to IgG control fraction (Figure 6C). To further investigate the mechanisms underlying HuR-mediated PPP1R3A regulation, in vitro-transcribed, biotinylated RNA fragments of the 5'UTR, CR (coding region), and 3'UTR of PPP1R3A mRNAs (Figure 6D) were used for RNA pull-down assays. HuR is associated with the PPP1R3A mRNA 3'UTRs, but not with other regions of the mRNA (Figure 6E). To test if the association of HuR with PPP1R3A mRNAs was functional, pGL3-derived reporters bearing fragments of PPP1R3A mRNAs were constructed (Figure 6F). Tendon cells were transfected with each of these reporters and 24 h later, they were transfected with siRNAs (control or HuR-directed) and cultured for an additional 48 h. Knock down of HuR reduced the luciferase activity of pGL3-derived vectors bearing the PPP1R3A 3'UTR but showed no effect on the activity of reporters bearing regions that did not interact with HuR (Figure 6G). Finally, we also tested the half-life of PPP1R3A mRNAs in tendon cells upon HuR silencing. Knock down of HuR caused an accelerated decline in PPP1R3A mRNA levels (Figure 6H) as evidence that PPP1R3A mRNA was less stable when HuR levels were diminished. As a control, the half-life of GAPDH mRNA was not altered by HuR-knockdown. Together, these results suggest that HuR regulates the expression of PPP1R3A by stabilizing its mRNA.

DISCUSSION

In this study, we investigated the role of PPP1R3A in calcific tendinopathy and identified a potential role of this regulatory unit in altering calcium deposition in tendon cells. PPP1R3A regulates intracellular calcium levels using the mechanosensory protein Piezo1 and SERCA2 in CT.

Calcific tendinopathy is a result of defective resorption of calcium crystals formed in tendonic regions, mainly in the rotator cuff region of the shoulders. The etiology of this disease is unknown, and a wide range of factors including mechanical stress and defective cellular pathways

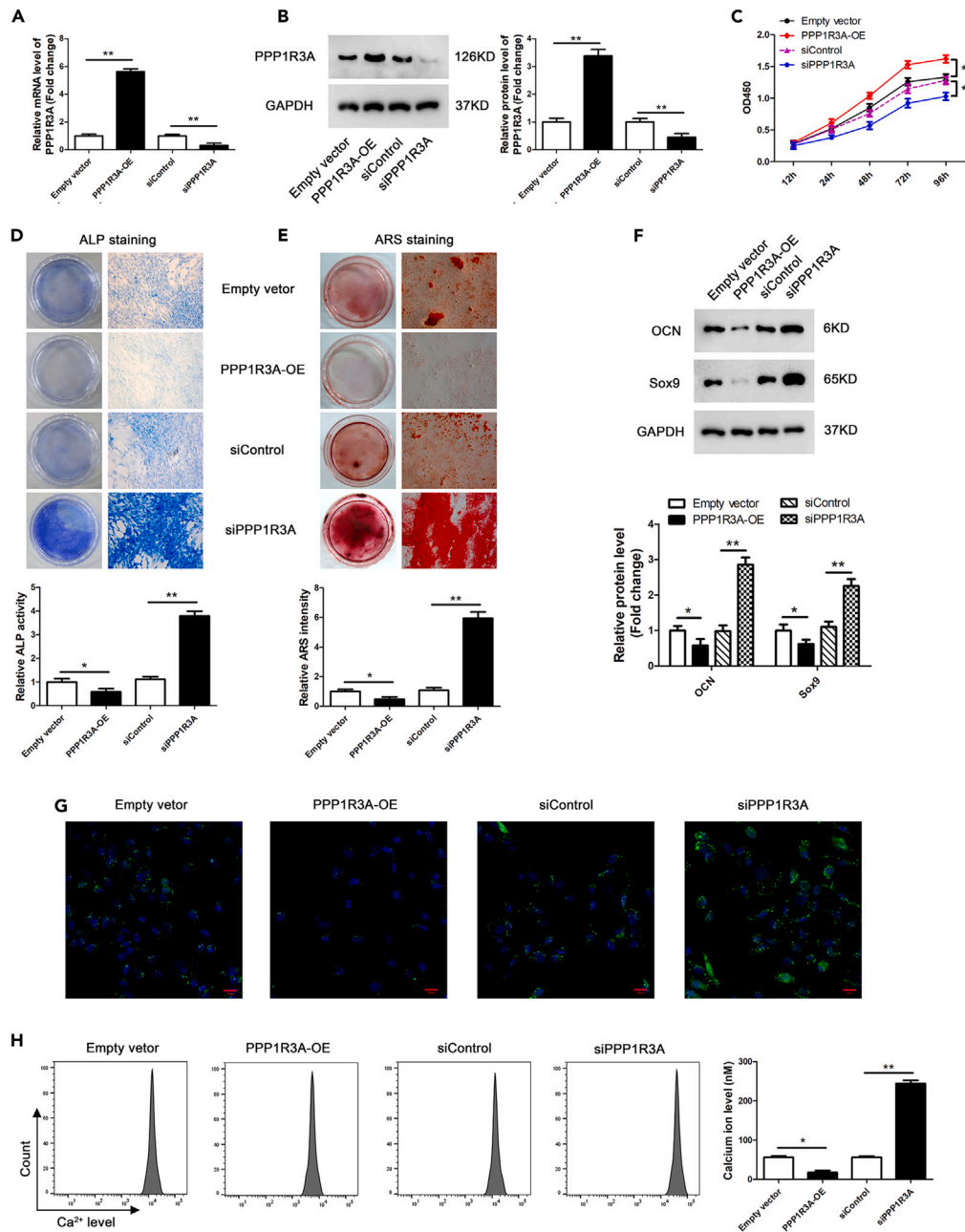


Figure 4. PPP1R3A regulates osteogenesis and intracellular Ca^{2+} level in tendon cells

(A) qRT-PCR analysis of PPP1R3A in tendon cells treated with PPP1R3A overexpression lentivirus or siRNA.

(B) Representative immunoblots and quantification of PPP1R3A protein expression in tendon cells.

(C) Cell proliferation assessed by CCK-8 assay for the different treatment groups.

(D) Representative images from alkaline phosphatase staining of tendon cells and ALP quantification on Day 7.

(E) Representative images from Alcian blue staining of tenocytes and ARS quantification on Day 14.

(F) Representative immunoblots and quantification of OCN and Sox9 in tendon cells cultured 7 days in the osteogenic medium. The densitometric values of the proteins were normalized to that of GAPDH.

(G) Visualization of the distribution of intracellular Ca^{2+} in tendon cells by Fluo-4AM Ca^{2+} fluorescence probe. Blue: cell nucleus stain, Green: intracellular Ca^{2+} .

(H) Quantification of intracellular Ca^{2+} levels by flow cytometry. Shown are representative histograms and quantification under different conditions. Results are shown as mean \pm SD of three independent repeats. * $p < 0.05$, ** $p < 0.01$. p value calculated was determined by two-tailed unpaired Student's t test.

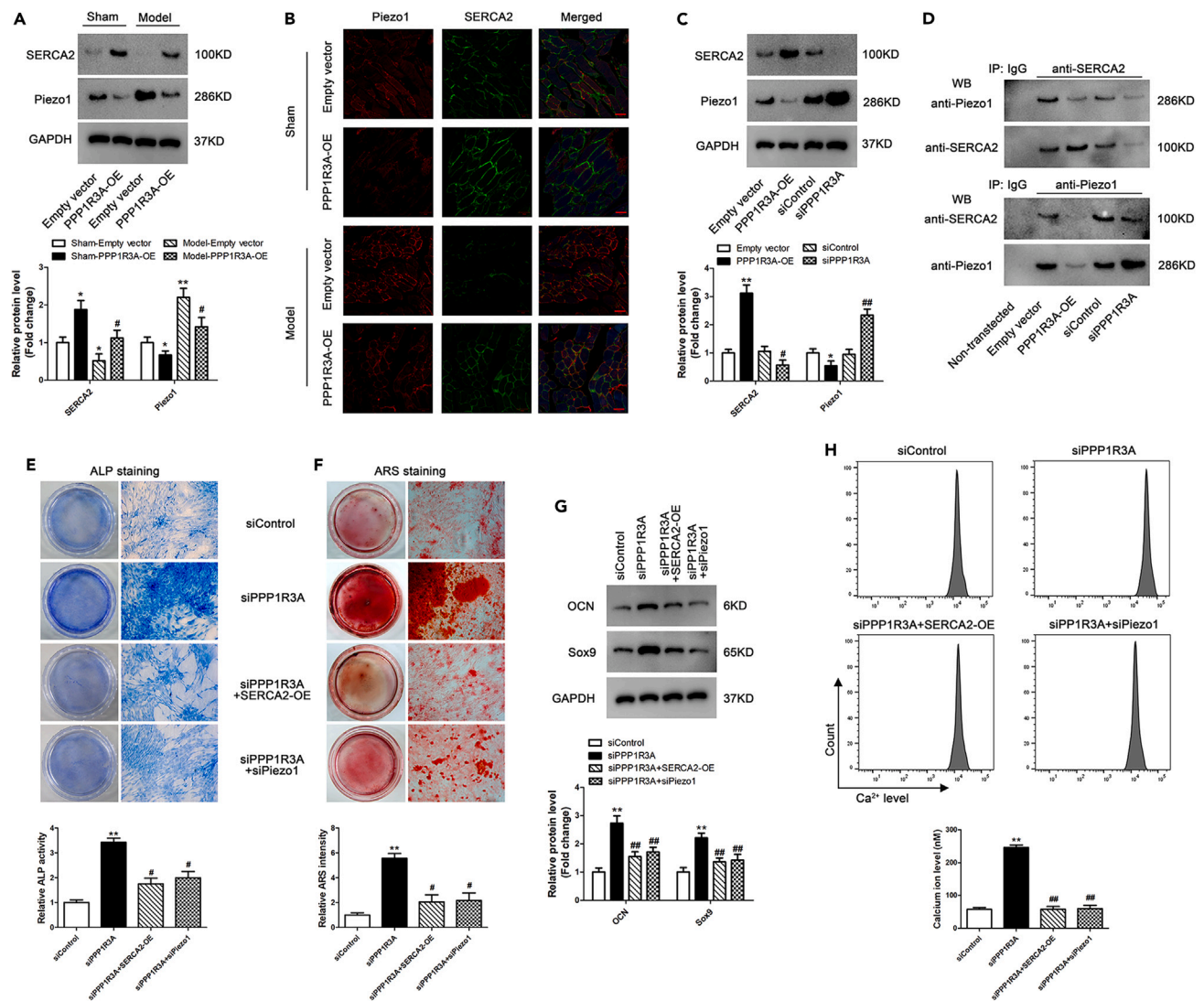


Figure 5. SERCA2/Piezo1 is involved in the regulation of osteogenesis and Ca^{2+} level in a PPP1R3A-dependent manner in tendon cells

(A) Representative immunoblots and densitometric quantification of Piezo1 and SERCA2 expression in rat Achilles tendons. The band intensity was normalized to GAPDH. Values are means \pm SD ($n = 6$). *, # $p < 0.05$, ** $p < 0.01$. * vs. the Sham-Empty vector group, # vs. the Model-Empty vector group. p value calculated was determined by two-tailed unpaired Student's t test.

(B) Representative micrographs of SERCA2 and Piezo1 expression in rat Achilles tendons visualized by immunofluorescence ($\times 400$; $n = 6$). Scale bars, 50 μ m.

(C) Representative immunoblots and densitometric quantification of Piezo1 and SERCA2 expression in tendon cells treated with PPP1R3A overexpression lentivirus or siRNA. $n = 3$ replicates for each group. p value calculated was determined by two-tailed unpaired Student's t test. *, # $p < 0.05$, **, ## $p < 0.01$. * vs. Empty vector, # vs. siControl.

(D and E) Representative immunoblots from co-immunoprecipitation experiments with antibodies against endogenous Piezo1, SERCA2 or control IgG in tendon cells treated with PPP1R3A overexpression lentivirus or siRNA (E) Representative images from alkaline phosphatase staining of tendon cells and ALP quantification on Day 7. $n = 3$ replicates for each group. p value calculated was determined by two-tailed unpaired Student's t test. ** $p < 0.01$, vs. Empty vector, # $p < 0.05$, vs. siControl.

(F) Representative images from alcian blue staining of tendon cells and ARS quantification on Day 14. $n = 3$ replicates for each group. p value calculated was determined by two-tailed unpaired Student's t test. ** $p < 0.01$, vs. Empty vector, # $p < 0.05$, vs. siControl.

(G) Representative immunoblots and corresponding densitometric quantification of OCN and Sox9 expression in tendon cells cultured for 3 days in the osteogenic medium. Protein expression was normalized to GAPDH. $n = 3$ replicates for each group. p value calculated was determined by two-tailed unpaired Student's t test. **, ## $p < 0.01$, * vs. Empty vector, # vs. siControl.

(H) Quantification of intracellular Ca^{2+} levels by flow cytometry. Shown are representative histograms and quantification under different conditions. Results are shown as mean \pm SD of at least three independent repeats. $n = 3$ replicates for each group. p value calculated was determined by two-tailed unpaired Student's t test. **, ## $p < 0.01$. * vs. siControl, # vs. siPPP1R3A.

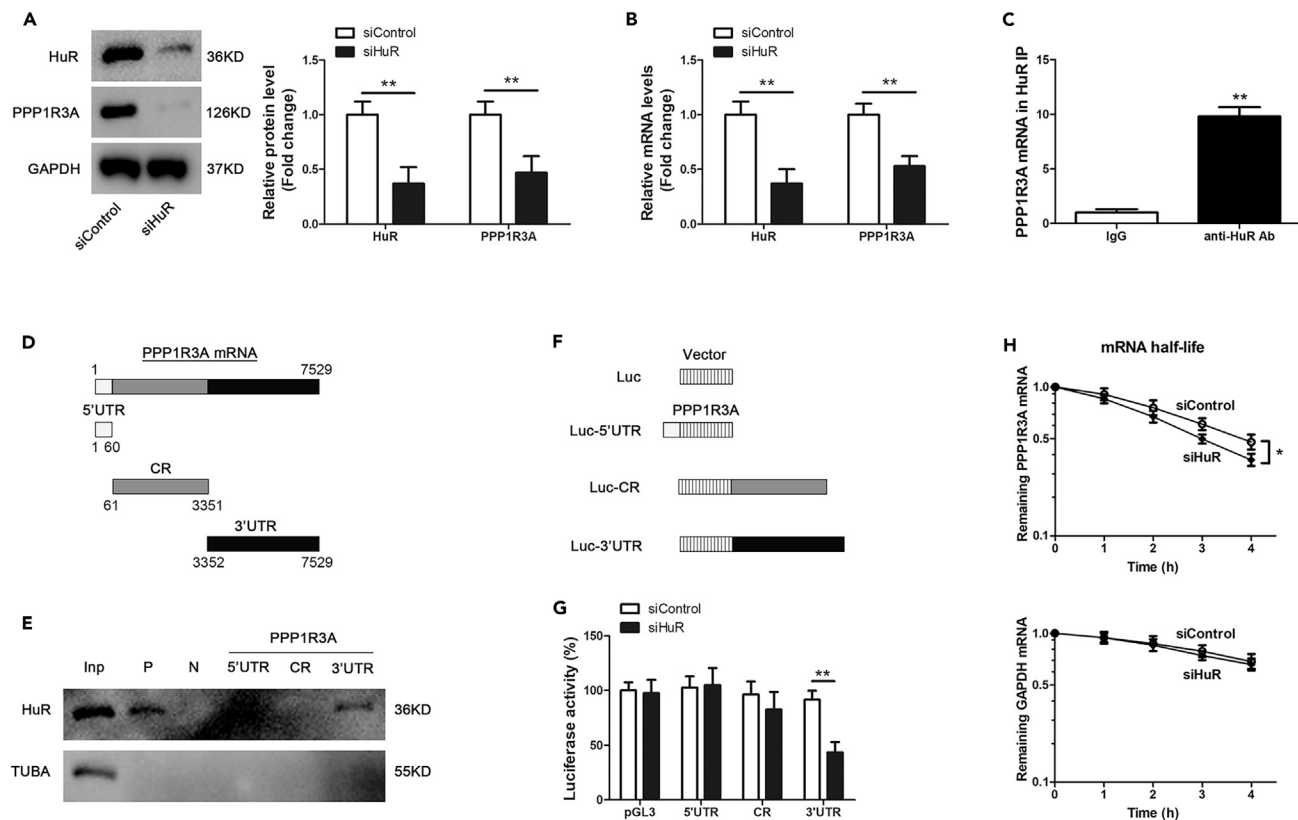


Figure 6. HuR interacts with PPP1R3A mRNA and increases its stability and translation in tendon cells

(A) Representative immunoblots and densitometric quantification of HuR and PPP1R3A expression in tendon cells treated with control or HuR siRNA. $n = 3$ replicates for each group. p value calculated was determined by two-tailed unpaired Student's t test. $**p < 0.01$.

(B) mRNA levels of HuR and PPP1R3A in tendon cells measured by qRT-PCR. $n = 3$ replicates for each group. p value calculated was determined by two-tailed unpaired Student's t test. $**p < 0.01$.

(C) RIP analysis to evaluate the association of endogenous HuR with endogenous PPP1R3A mRNA. Quantification of PPP1R3A by RT-qPCR analysis in immunoprecipitated fractions using either anti-HuR antibody or control IgG in tendon cells. Values are the means \pm SD from triplicate samples. $n = 3$ replicates for each group. p value calculated was determined by two-tailed unpaired Student's t test. $**p < 0.01$ compared with IgG IP.

(D and E) Schematic representation of the different regions in PPP1R3A mRNAs used for RNA pull-down assays (E) Immunoblots probed for HuR and control TUBA from different biotinylated pull-down fractions: PPP1R3A 5'-UTR, CR (coding region), and 3'-UTR. p27 5'UTR and CR served as positive (P) and negative (N) controls, respectively. α -Tubulin (TUBA) as the internal control.

(F and G) Schematic representation of the different pGL3-derived reporter vectors generated bearing the PPP1R3A mRNA fragments for luciferase assay (G) Luciferase activity in tendon cells. Cells were transfected with siControl or siHuR for 24 h. Cells were subsequently transfected with each of the pGL3-derived reporters together with a pRL-CMV vector and cultured for an additional 48 h. Luciferase activity was measured by a luminometer. $n = 3$ replicates for each group. p value calculated was determined by two-tailed unpaired Student's t test. $**p < 0.01$.

(H) Half-lives of PPP1R3A and GAPDH mRNAs were examined at different time points post actinomycin D treatment in siControl or siHuR transfected tendon cells. p value calculated was determined by two-tailed unpaired Student's t test. $*p < 0.05$ compared with siControl. Results are shown as mean \pm SD of three independent repeats.

have been suggested to contribute toward the development of CT.³⁴ By comparing gene expression data from tendinopathy patients and healthy adults from a previously described study,²⁰ we identified that PPP1R3A was downregulated in tendinopathy. Furthermore, using tendon cells from an *in vivo* mouse model for calcific tendinopathy, we were able to rescue the pathological effects by PPP1R3A overexpression *ex vivo*. Our results indicated that the described role for protein phosphatase may as a potential protector in tendinitis. Previously, alkaline phosphatases have been shown to promote calcium deposition and tendinitis, having a negative role in tenocyte regulation.¹³ Expression of non-specific alkaline phosphatase (TNAP) and ectonucleotide pyrophosphatase/phosphodiesterase 1 (ENPP1) were highly expressed in calcific regions and using an alkaline phosphatase inhibitor prevented deposition of minerals. A study by Ho et al., showed that mice with a mutation in the *Ank* gene (progressive ankylosis locus) developed arthritis-like symptoms that involved mineral deposition and tendon degeneration.³⁵ *Ank* encodes for a transporter protein that transports inorganic pyrophosphates (PPi) out of cells. Reducing the secretion of PPis reduced calcification *in vivo* in mice. Later, another study showed that TNAP also contributes toward calcification, together with ANK, by regulating PPi levels.³⁶

Low levels of PPP1R3A resulted in the upregulation of osteo/chondrogenic markers and increase in intracellular Ca²⁺ deposition. These are characteristics of tendinopathy development as described by several studies from clinical samples that show presence of cells expressing high levels of OCN and Sox9 in the vicinity of mineral deposition in tendon tissues.^{14,37} The observed increase in osteo/chondrogenic markers as a result of tendinopathy in our *in vivo* rat model was similar to observations in other rat models of tendinopathy.³⁸

Piezo1 is a mechanosensitive channel that is regulated by the Ca²⁺-dependent ATPase SERCA2.³² In Achilles tendon tissues, reduction in PPP1R3A levels resulted in a higher expression of Piezo1 and lower levels of SERCA2. Deregulation of Piezo1 and SERCA2 expression may be a direct cause of accumulation of intracellular calcium deposits. Previously, deregulation in SERCA2 expression and intracellular Ca²⁺ levels has been widely studied in cardiomyocytes.^{39,40} SERCA2 activity is required for the removal of Ca²⁺ during cardiomyocyte relaxation. Its affinity for Ca²⁺ plays a major role in cardiomyocyte regulation, as higher affinity can result in cardiac hypertrophy.⁴¹ Therefore, evaluating the sensitivity of SERCA2 to Ca²⁺ in tendon cells will give insights into how this protein regulates calcium deposition during the formative and resorptive phases of CT.

Ca²⁺ homeostasis is a process of dynamic balance between Ca²⁺ stores and Ca²⁺ releases. As the largest intracellular Ca²⁺ reservoir, the SR/ER is an extensive, dynamic, and highly heterogeneous membranous structure that caters to various homeostatic functions including keeping Ca²⁺ homeostasis.²¹ Ca²⁺ release from SR/ER stores to the cytosol is a spontaneous reaction due to the huge concentration difference between both cell spaces. Contrary to Ca²⁺ release, SR/ER refilling needs to expend energy against the concentration gradient. SERCA is the main transporter that takes part in this process, pumping two Ca²⁺ ions back to the SR/ER lumen at the cost of consuming one ATP molecule. Inhibition of SERCA can lead to Ca²⁺ retention in the cytosol and then higher intracellular calcium concentration. According to the experimental results, it was assumed that reduction in PPP1R3A levels in tendon cells resulted in the inhibition of SERCA2 and abnormal Ca²⁺ release from the ER into the cytosol to activate the Piezo1 channel, which can cause Ca²⁺ to flow into extracellular space, ultimately leading to extracellular calcium deposition in tendon tissues. Deregulation in intracellular Ca²⁺ levels is evidence that the calcium balance of the tendon cell itself is disrupted directly. Further experiments are needed to verify the Ca²⁺ flow from the cytosol to extracellular space in the tendon.

The expression of PPP1R3A was regulated by HuR. HuR is an RNA-binding protein that was described in *Drosophila* as an embryonic lethal abnormal vision (ELAV) family of Hu proteins. It acts at the posttranscriptional level by regulating the stability and translation of mRNA.⁴² By interacting with RNAs and altering their expression patterns, it regulates adipogenesis and plays an important role in cardiovascular diseases.^{43,44} Therefore, in addition to regulation of PPP1R3A expression in the context of CT, HuR may also regulate other RNAs that affect tendon cell differentiation and survival.

Limitations of the study

In this study, the isolated tendon cells were a mixture of cells, including tendon-derived stem cells, tenocytes, tenoblasts, and fibroblasts. This may be a limitation of the study that the presence of specific cells could not be confirmed due to the lack of specific recognized markers for each type of cells. Evidence shows that besides tendon stem cells, tenocytes also possess the intrinsic potential to transdifferentiate into non-tenocytes, which both cells may be involved in tendon degeneration such as calcification. Of note, in physiological conditions the complex interactions of multiple cells are involved in the tissue response to external stimuli, leading to pathologic changes. We believe that metaplasia, which is the aberrant differentiation of tissues, cannot be driven by a single cell type, and that was a consequence of the interaction of multiple cells. Although a miscellaneous collection of cells was used in our study, our results were still valid.

Besides, in our study, the phenotypic properties of tendon tissues in sham groups have no significant change, the tendon structures were similar to the normal tendon. As shown in the Model-empty vector group, we have established a calcified tendinopathy animal model with key features of tendinopathy observed clinically and showing chondrocyte phenotype and ectopic ossification. Although, for the rigor of the experiment, a blank control should be set, we believe that the use of an empty vector did not significantly influence our results. Nonetheless, further studies would be typically subjected to more stringent requirements in setting up experimental groups.

Conclusion

Based on our results, we propose a model where regulation of PPP1R3A expression by HuR renders tendon cells sensitive to Ca²⁺ changes through Piezo1/SERCA2 in the context of CT. Our study identifies PPP1R3A as a potential therapeutic target for the treatment of CT.

STAR★METHODS

Detailed methods are provided in the online version of this paper and include the following:

- KEY RESOURCES TABLE
- RESOURCE AVAILABILITY
 - Lead contact
 - Materials availability
 - Data and code availability
- EXPERIMENTAL MODEL AND STUDY PARTICIPANT DETAILS
 - Animal experiments
 - Patients and tissues samples
 - Primary rat tendon cell isolation and culture

● **METHOD DETAILS**

- Gene expression dataset
- Histology, immunohistochemistry, and immunofluorescence assays
- Reconstruction of plasmids and lentivirus packing
- siRNA transfection
- Quantitative real-time PCR
- Western blot analysis
- Cell proliferation assay
- Cell osteogenic differentiation induction
- Alkaline phosphatase activity and alizarin red-S staining
- Cytosolic Ca²⁺ measurement
- Calcium ion detection
- RNA immunoprecipitation (RIP) analysis
- Biotin pull-down assays
- Luciferase reporter assay
- RNA half-life analysis

● **QUANTIFICATION AND STATISTICAL ANALYSIS**

SUPPLEMENTAL INFORMATION

Supplemental information can be found online at <https://doi.org/10.1016/j.isci.2023.107784>.

ACKNOWLEDGMENTS

This work was supported by the Sports injury repair and reconstruction research innovation group (cstc2020jcyj-cxttX0004), the National Natural Science Foundation of China (82130071) and the Top Talent Support Program for young and middle-aged people of Wuxi Health Committee.

AUTHOR CONTRIBUTIONS

T.K.-L. and H.C. conceived and designed the research, analyzed and interpreted the data, and wrote and revised the manuscript. H.C., M.L., G.S., Y.M.-Y., M.M.-D., and C.L. designed and performed the *in vivo* experiments. H.P., Y.X., W.W., T.X., Z.W.-H., and C.W. performed and analyzed *in vitro* experiments.

DECLARATION OF INTERESTS

The authors declare no competing interests.

INCLUSION AND DIVERSITY

We support inclusive, diverse, and equitable conduct of research.

Received: March 13, 2023

Revised: July 25, 2023

Accepted: August 28, 2023

Published: August 30, 2023

REFERENCES

1. Depalma, A.F., and Kruper, J.S. (1961). Long-term study of shoulder joints afflicted with and treated for calcific tendinitis. *Clin. Orthop.* 20, 61–72.
2. Catapano, M., Robinson, D.M., Schowalter, S., and McInnis, K.C. (2022). Clinical evaluation and management of calcific tendinopathy: an evidence-based review. *J. Osteopath. Med.* 122, 141–151. <https://doi.org/10.1515/jom-2021-0213>.
3. Sansone, V., Maiorano, E., Galluzzo, A., and Pascale, V. (2018). Calcific tendinopathy of the shoulder: clinical perspectives into the mechanisms, pathogenesis, and treatment. *Orthop. Res. Rev.* 10, 63–72. <https://doi.org/10.2147/ORR.S138225>.
4. Merolla, G., Bhat, M.G., Paladini, P., and Porcellini, G. (2015). Complications of calcific tendinitis of the shoulder: a concise review. *J. Orthop. Traumatol.* 16, 175–183. <https://doi.org/10.1007/s10195-015-0339-x>.
5. Kim, M.S., Kim, I.W., Lee, S., and Shin, S.J. (2020). Diagnosis and treatment of calcific tendinitis of the shoulder. *Clin. Shoulder Elb.* 23, 210–216. <https://doi.org/10.5397/cise.2020.00318>.
6. Benjamin, M., Rufai, A., and Ralphs, J.R. (2000). The mechanism of formation of bony spurs (enthesophytes) in the achilles tendon. *Arthritis Rheum.* 43, 576–583. [https://doi.org/10.1002/1529-0131\(200003\)43:3<576::AID-ANR14>3.0.CO;2-A](https://doi.org/10.1002/1529-0131(200003)43:3<576::AID-ANR14>3.0.CO;2-A).
7. Tashjian, R.Z. (2012). Epidemiology, natural history, and indications for treatment of rotator cuff tears. *Clin. Sports Med.* 31, 589–604. <https://doi.org/10.1016/j.csm.2012.07.001>.
8. Gumina, S., Candela, V., Passaretti, D., Latino, G., Venditto, T., Mariani, L., and Santilli, V. (2014). The association between body fat and rotator cuff tear: the influence on rotator cuff tear sizes. *J. Shoulder Elbow Surg.* 23, 1669–1674. <https://doi.org/10.1016/j.jse.2014.03.016>.
9. Foolen, J., Wunderli, S.L., Loerakker, S., and Snedeker, J.G. (2018). Tissue alignment enhances remodeling potential of tendon-derived cells - Lessons from a novel

- microtissue model of tendon scarring. *Matrix Biol.* 65, 14–29. <https://doi.org/10.1016/j.matbio.2017.06.002>.
10. Corps, A.N., Jones, G.C., Harrall, R.L., Curry, V.A., Hazleman, B.L., and Riley, G.P. (2008). The regulation of aggrecanase ADAMTS-4 expression in human Achilles tendon and tendon-derived cells. *Matrix Biol.* 27, 393–401. <https://doi.org/10.1016/j.matbio.2008.02.002>.
 11. Zhang, J., and Wang, J.H.C. (2010). Production of PGE(2) increases in tendons subjected to repetitive mechanical loading and induces differentiation of tendon stem cells into non-tenocytes. *J. Orthop. Res.* 28, 198–203. <https://doi.org/10.1002/jor.20962>.
 12. Zhang, J., and Wang, J.H.C. (2010). Mechanobiological response of tendon stem cells: implications of tendon homeostasis and pathogenesis of tendinopathy. *J. Orthop. Res.* 28, 639–643. <https://doi.org/10.1002/jor.21046>.
 13. Darrieurt-Laffite, C., Arnolfo, P., Garraud, T., Adrait, A., Couté, Y., Louarn, G., Trichet, V., Layrolle, P., Le Goff, B., and Blanchard, F. (2019). Rotator Cuff Tenocytes Differentiate into Hypertrophic Chondrocyte-Like Cells to Produce Calcium Deposits in an Alkaline Phosphatase-Dependent Manner. *J. Clin. Med.* 8, 1544. <https://doi.org/10.3390/jcm8101544>.
 14. Archer, R.S., Bayley, J.I., Archer, C.W., and Ali, S.Y. (1993). Cell and matrix changes associated with pathological calcification of the human rotator cuff tendons. *J. Anat.* 182, 1–11.
 15. Yamamoto, K., Hojo, H., Koshima, I., Chung, U.I., and Ohba, S. (2012). Famotidine suppresses osteogenic differentiation of tendon cells in vitro and pathological calcification of tendon in vivo. *J. Orthop. Res.* 30, 1958–1962. <https://doi.org/10.1002/jor.22146>.
 16. Westphal, R.S., Tavalin, S.J., Lin, J.W., Alto, N.M., Fraser, I.D., Langeberg, L.K., Sheng, M., and Scott, J.D. (1999). Regulation of NMDA receptors by an associated phosphatase-kinase signaling complex. *Science* 285, 93–96. <https://doi.org/10.1126/science.285.5424.93>.
 17. Alsina, K.M., Hulsurkar, M., Brandenburg, S., Kownatzki-Danger, D., Lenz, C., Urlaub, H., Abu-Taha, I., Kamler, M., Chiang, D.Y., Lahiri, S.K., et al. (2019). Loss of Protein Phosphatase 1 Regulatory Subunit PPP1R3A Promotes Atrial Fibrillation. *Circulation* 140, 681–693. <https://doi.org/10.1161/CIRCULATIONAHA.119.039642>.
 18. Liu, X., Shiwaku, Y., Hamai, R., Tsuchiya, K., Takahashi, T., and Suzuki, O. (2023). Effect of Octacalcium Phosphate Crystals on the Osteogenic Differentiation of Tendon Stem/Progenitor Cells In Vitro. *Int. J. Mol. Sci.* 24, 1235. <https://doi.org/10.3390/ijms24021235>.
 19. Li, H., Korcari, A., Ciufo, D., Mendias, C.L., Rodeo, S.A., Buckley, M.R., Loiselle, A.E., Pitt, G.S., and Cao, C. (2023). Increased Ca(2+) signaling through Ca(V) 1.2 induces tendon hypertrophy with increased collagen fibrillogenesis and biomechanical properties. *Faseb. J.* 37, e23007. <https://doi.org/10.1096/fj.202300607R>.
 20. Jelinsky, S.A., Rodeo, S.A., Li, J., Gulotta, L.V., Archambault, J.M., and Seeherman, H.J. (2011). Regulation of gene expression in human tendinopathy. *BMC Musculoskel. Disord.* 12, 86. <https://doi.org/10.1186/1471-2474-12-86>.
 21. Bravo-Sagua, R., Parra, V., Muñoz-Cordova, F., Sanchez-Aguilera, P., Garrido, V., Contreras-Ferrat, A., Chiong, M., and Lavandero, S. (2020). Sarcoplasmic reticulum and calcium signaling in muscle cells: Homeostasis and disease. *Int. Rev. Cell Mol. Biol.* 350, 197–264. <https://doi.org/10.1016/bs.ircmb.2019.12.007>.
 22. Hetz, C., and Papa, F.R. (2018). The Unfolded Protein Response and Cell Fate Control. *Mol. Cell* 69, 169–181. <https://doi.org/10.1016/j.molcel.2017.06.017>.
 23. Park, S.J., Li, C., and Chen, Y.M. (2021). Endoplasmic Reticulum Calcium Homeostasis in Kidney Disease: Pathogenesis and Therapeutic Targets. *Am. J. Pathol.* 191, 256–265. <https://doi.org/10.1016/j.ajpath.2020.11.006>.
 24. Halder, D., Jeon, S.J., Yoon, J.Y., Lee, J.J., Jun, S.Y., Choi, M.H., Jeong, B., Sung, D.H., Lee, D.Y., Kim, B.J., and Kim, N.S. (2022). TREX1 Deficiency Induces ER Stress-Mediated Neuronal Cell Death by Disrupting Ca(2+) Homeostasis. *Mol. Neurobiol.* 59, 1398–1418. <https://doi.org/10.1007/s12035-021-02631-3>.
 25. Fu, X., Cui, J., Meng, X., Jiang, P., Zheng, Q., Zhao, W., and Chen, X. (2021). Endoplasmic reticulum stress, cell death and tumor: Association between endoplasmic reticulum stress and the apoptosis pathway in tumors (Review). *Oncol. Rep.* 45, 801–808. <https://doi.org/10.3892/or.2021.7933>.
 26. Britzolaki, A., Saurine, J., Flaherty, E., Thelen, C., and Pitychoutis, P.M. (2018). The SERCA2: A Gatekeeper of Neuronal Calcium Homeostasis in the Brain. *Cell. Mol. Neurobiol.* 38, 981–994. <https://doi.org/10.1007/s10571-018-0583-8>.
 27. Vangheluwe, P., Sipido, K.R., Raeymaekers, L., and Wuytack, F. (2006). New perspectives on the role of SERCA2's Ca²⁺ affinity in cardiac function. *Biochim. Biophys. Acta* 1763, 1216–1228. <https://doi.org/10.1016/j.bbamcr.2006.08.025>.
 28. Coste, B., Mathur, J., Schmidt, M., Earley, T.J., Ranade, S., Petrus, M.J., Dubin, A.E., and Patapoutian, A. (2010). Piezo1 and Piezo2 are essential components of distinct mechanically activated cation channels. *Science* 330, 55–60. <https://doi.org/10.1126/science.1193270>.
 29. Xu, X., Liu, S., Liu, H., Ru, K., Jia, Y., Wu, Z., Liang, S., Khan, Z., Chen, Z., Qian, A., and Hu, L. (2021). Piezo Channels: Awesome Mechanosensitive Structures in Cellular Mechanotransduction and Their Role in Bone. *Int. J. Mol. Sci.* 22, 6429. <https://doi.org/10.3390/ijms22126429>.
 30. Lee, W., Leddy, H.A., Chen, Y., Lee, S.H., Zelenski, N.A., McNulty, A.L., Wu, J., Becker, K.N., Coles, J., Zauscher, S., et al. (2014). Synergy between Piezo1 and Piezo2 channels confers high-strain mechanosensitivity to articular cartilage. *Proc. Natl. Acad. Sci. USA* 111, E5114–E5122. <https://doi.org/10.1073/pnas.1414298111>.
 31. Servin-Vences, M.R., Moroni, M., Lewin, G.R., and Poole, K. (2017). Direct measurement of TRPV4 and PIEZO1 activity reveals multiple mechanotransduction pathways in chondrocytes. *Elife* 6, e21074. <https://doi.org/10.7554/eLife.21074>.
 32. Zhang, T., Chi, S., Jiang, F., Zhao, Q., Xiao, B., and Xiao, B. (2017). A protein interaction mechanism for suppressing the mechanosensitive Piezo channels. *Nat. Commun.* 8, 1797. <https://doi.org/10.1038/s41467-017-01712-z>.
 33. Qiu, X., Deng, Z., Wang, M., Feng, Y., Bi, L., and Li, L. (2023). Piezo protein determines stem cell fate by transmitting mechanical signals. *Hum. Cell* 36, 540–553. <https://doi.org/10.1007/s13577-022-00853-8>.
 34. Darrieurt-Laffite, C., Blanchard, F., and Le Goff, B. (2018). Calcific tendonitis of the rotator cuff: From formation to resorption. *Joint Bone Spine* 85, 687–692. <https://doi.org/10.1016/j.jbspin.2017.10.004>.
 35. Ho, A.M., Johnson, M.D., and Kingsley, D.M. (2000). Role of the mouse ank gene in control of tissue calcification and arthritis. *Science* 289, 265–270. <https://doi.org/10.1126/science.289.5477.265>.
 36. Peach, C.A., Zhang, Y., Dunford, J.E., Brown, M.A., and Carr, A.J. (2007). Cuff tear arthropathy: evidence of functional variation in pyrophosphate metabolism genes. *Clin. Orthop. Relat. Res.* 462, 67–72. <https://doi.org/10.1097/BLO.0b013e31811f39de>.
 37. Uthoff, H.K., Sarkar, K., and Maynard, J.A. (1976). Calcifying tendinitis: a new concept of its pathogenesis. *Clin. Orthop. Relat. Res.* 164–168.
 38. Archambault, J.M., Jelinsky, S.A., Lake, S.P., Hill, A.A., Glaser, D.L., and Soslowky, L.J. (2007). Rat supraspinatus tendon expresses cartilage markers with overuse. *J. Orthop. Res.* 25, 617–624. <https://doi.org/10.1002/jor.20347>.
 39. Hu, L.Y.R., Ackermann, M.A., Hecker, P.A., Prosser, B.L., King, B., O'Connell, K.A., Grogan, A., Meyer, L.C., Berndsen, C.E., Wright, N.T., et al. (2017). Deregulated Ca(2+) cycling underlies the development of arrhythmia and heart disease due to mutant obscurin. *Sci. Adv.* 3, e1603081. <https://doi.org/10.1126/sciadv.1603081>.
 40. Kumarswamy, R., Lyon, A.R., Volkman, I., Mills, A.M., Bretthauer, J., Pahuja, A., Geers-Knorr, C., Kraft, T., Hajjar, R.J., Macleod, K.T., et al. (2012). SERCA2a gene therapy restores microRNA-1 expression in heart failure via an Akt/FoxO3A-dependent pathway. *Eur. Heart J.* 33, 1067–1075. <https://doi.org/10.1093/eurheartj/ehs043>.
 41. Vangheluwe, P., Tjwa, M., Van Den Bergh, A., Louch, W.E., Beullens, M., Dode, L., Carmeliet, P., Kranias, E., Herijgers, P., Sipido, K.R., et al. (2006). A SERCA2 pump with an increased Ca²⁺ affinity can lead to severe cardiac hypertrophy, stress intolerance and reduced life span. *J. Mol. Cell. Cardiol.* 41, 308–317. <https://doi.org/10.1016/j.yjmcc.2006.05.014>.
 42. Xiao, L., Li, X.X., Chung, H.K., Kalakonda, S., Cai, J.Z., Cao, S., Chen, N., Liu, Y., Rao, J.N., Wang, H.Y., et al. (2019). RNA-Binding Protein HuR Regulates Paneth Cell Function by Altering Membrane Localization of TLR2 via Post-transcriptional Control of CNPY3. *Gastroenterology* 157, 731–743. <https://doi.org/10.1053/j.gastro.2019.05.010>.
 43. Siang, D.T.C., Lim, Y.C., Kyaw, A.M.M., Win, K.N., Chia, S.Y., Degirmenci, U., Hu, X., Tan, B.C., Walet, A.C.E., Sun, L., and Xu, D. (2020). The RNA-binding protein HuR is a negative regulator in adipogenesis. *Nat. Commun.* 11, 213. <https://doi.org/10.1038/s41467-019-14001-8>.
 44. Rajasingh, J. (2015). The many facets of RNA-binding protein HuR. *Trends Cardiovasc. Med.* 25, 684–686. <https://doi.org/10.1016/j.tcm.2015.03.013>.
 45. Chen, Y., Xie, Y., Liu, M., Hu, J., Tang, C., Huang, J., Qin, T., Chen, X., Chen, W., Shen, W., and Yin, Z. (2019). Controlled-release curcumin attenuates progression of tendon

- ectopic calcification by regulating the differentiation of tendon stem/progenitor cells. *Mater. Sci. Eng. C* 103, 109711. <https://doi.org/10.1016/j.msec.2019.04.090>.
46. Wu, Y.F., Huang, Y.T., Wang, H.K., Yao, C.C.J., Sun, J.S., and Chao, Y.H. (2017). Hyperglycemia Augments the Adipogenic Transdifferentiation Potential of Tenocytes and Is Alleviated by Cyclic Mechanical Stretch. *Int. J. Mol. Sci.* 19, 90. <https://doi.org/10.3390/ijms19010090>.
47. Hsiao, M.Y., Lin, P.C., Liao, W.H., Chen, W.S., Hsu, C.H., He, C.K., Wu, Y.W., Gefen, A., Iafisco, M., Liu, L., and Lin, F.H. (2019). The Effect of the Repression of Oxidative Stress on Tenocyte Differentiation: A Preliminary Study of a Rat Cell Model Using a Novel Differential Tensile Strain Bioreactor. *Int. J. Mol. Sci.* 20, 3437. <https://doi.org/10.3390/ijms20143437>.
48. Hu, H., Jiang, M., Cao, Y., Zhang, Z., Jiang, B., Tian, F., Feng, J., Dou, Y., Gorospe, M., Zheng, M., et al. (2020). HuR regulates phospholamban expression in isoproterenol-induced cardiac remodelling. *Cardiovasc. Res.* 116, 944–955. <https://doi.org/10.1093/cvr/cvz205>.

STAR★METHODS

KEY RESOURCES TABLE

REAGENT or RESOURCE	SOURCE	IDENTIFIER
Antibodies		
Rabbit polyclonal anti-PPP1R3A	This paper	N/A
Rabbit monoclonal anti-Collagen I	Abcam	Cat# ab270993, RRID:AB_2927551
Rabbit polyclonal anti-TNMD	This paper	N/A
Mouse monoclonal anti-osteocalcin (D-11)	Santa Cruz Biotechnology	Cat# sc-390877, RRID:AB_2937079
Mouse monoclonal anti-Sox9 (E-9)	Santa Cruz Biotechnology	Cat# sc-166505, RRID:AB_2255399
Mouse monoclonal anti-SERCA2 (F-1)	Santa Cruz Biotechnology	Cat# sc-376235, RRID:AB_10989947
Rabbit polyclonal anti-Piezo1	Proteintech	Cat# 15939-1-AP, RRID:AB_2231460
Rabbit monoclonal anti-HuR/ELAVL1	Abcam	Cat# ab200342, RRID:AB_2784506
Mouse monoclonal anti-GAPDH (G-9)	Santa Cruz Biotechnology	Cat# sc-365062, RRID:AB_10847862
Mouse monoclonal anti- alpha Tubulin (TU-02)	Santa Cruz Biotechnology	Cat# sc-8035, RRID:AB_628408
HRP-labeled Goat anti-Rabbit IgG (H + L)	Beyotime	Cat# A0208, RRID:AB_2892644
HRP-labeled goat anti-mouse IgG (H + L)	Beyotime	Cat# A0216, RRID:AB_2860575
Bacterial and virus strains		
pCDH-CMV-MCS-EF1-copGFP	System Biosciences	N/A
pCDH-CMV-PPP1R3A-EF1-copGFP	System Biosciences	N/A
Biological samples		
Human calcific tendon and adjacent normal tendon tissue	This paper	N/A
Chemicals, peptides, and recombinant proteins		
Type I collagenase	Gibco	17100017
Alizarin Red Staining Solution	Sigma-Aldrich	TMS-008
Cetylpyridinium chloride	Sigma-Aldrich	C0732-100G
Pluronic F 127	Beyotime	ST501-0.1g
Fluo-4 a.m.	Beyotime	S1060
Dynabeads™ M-280 streptavidin	Invitrogen	11205D
actinomycin D	Sigma-Aldrich	SBR00013
Critical commercial assays		
Cell Counting Kit-8 (CCK-8 Kit)	Beyotime	C0038
BCIP/NBT color kit	Nanjing Jiancheng Bioengineering Institute	I023-1-1
Alkaline Phosphatase Assay Kit	Beyotime	P0321S
Dual-Luciferase® Reporter Assay System	Promega	E1910
Magna RIP ® RNA Binding Protein immunoprecipitation Kit	Millipore	17-700
Deposited data		
Raw and analyzed data	Jelinsky et al. ²⁰	GSM 26051
Experimental models: Cell lines		
Primary rat tendon cells	This paper	N/A
Experimental models: Organisms/strains		
SD rat: Collagenase I-induced tendon calcification	Chen et al. ⁴⁵	N/A

(Continued on next page)

Continued

REAGENT or RESOURCE	SOURCE	IDENTIFIER
Oligonucleotides		
siRNA targeting sequences: rat PPP1R3A #1–3, see Table S1	This paper	N/A
siRNA targeting sequences: rat Piezo1 #1–3, see Table S1	This paper	N/A
siRNA targeting sequences: rat HuR #1–3, see Table S1	This paper	N/A
siRNA targeting sequences: non-specific negative control, see Table S1	This paper	N/A
Primers for RT-qPCR, see Table S2	This paper	N/A
Primers for Biotin pull-down Assays, see Table S3	This paper	N/A
Primers for pGL3-PPP1R3A reporter vectors, see Table S4	This paper	N/A
Recombinant DNA		
pGL3-promoter vector	Promega	E1761
Plasmid: pGL3-PPP1R3A 5'-UTR	This paper	N/A
Plasmid: pGL3-PPP1R3A CR	This paper	N/A
Plasmid: pGL3-PPP1R3A 3'-UTR	This paper	N/A
pRL-CMV vector	Promega	E2261
Software and algorithms		
GraphPad Prism 5	GraphPad Software	RRID:SCR_002798 https://www.graphpad.com/
Other		
Nikon A1R MP Confocal Microscope	Nikon	RRID:SCR_020319
SpectraMax 190 microplate reader	Molecular Devices	RRID:SCR_018932
Zeiss LSM 510 META confocal microscope	Carl Zeiss AG	RRID:SCR_018062

RESOURCE AVAILABILITY

Lead contact

Further information and requests for resources and reagents should be directed to and will be fulfilled by the lead contact, Kang-Lai Tang (tangkanglai@hotmail.com).

Materials availability

This study did not generate new unique reagents.

Data and code availability

- This paper analyzes existing, publicly available data. These accession numbers for the datasets are listed in the [key resources table](#). All data reported in this paper will be shared by the [lead contact](#) upon request.
- This paper does not report original code.
- Any additional information required to reanalyze the data reported in this paper is available from the [lead contact](#) upon request.

EXPERIMENTAL MODEL AND STUDY PARTICIPANT DETAILS

Animal experiments

Animal experiments were conducted with the approval of the Army Medical University Experimental Animal Welfare and Ethics Committee (Army Medical University). All experiments with animals were carried according to Experimental Safety of Chinese Academy of Sciences and the Committees of Animal Ethics. All animal treatments were performed according to the guidelines provided by National Institutes of Health (NIH). Male 8-week-old Sprague-Dawley (SD) rats ($n = 6/\text{group}$) were used in this experiment. All rats were randomly assigned to four groups: (1) Sham (saline injection) + Empty vector (control lentivirus injection), (2) Sham + PPP1R3A-OE (PPP1R3A-overexpressing lentivirus injection), (3) Model (Type I collagenase injection) + Empty vector, (4) Model + PPP1R3A-OE. Rats were anesthetized using 2.5% pentobarbital sodium (0.25 mL/100 g body weight). Collagenase I-induced tendon calcification rat model was established as described before.⁴⁵ Briefly, Type I

collagenase (50 U/leg, Gibco, 17100017) or saline was injected into the midpoint of the Achilles tendons. Three days later, 50 μ L PPP1R3A-overexpressing lentivirus (1×10^9 TU/ml) or control lentivirus (System Biosciences, SBI, Palo Alto, CA, USA) was injected into the same injection site once as before. After 12 weeks, rats from each group were euthanized to harvest tendon tissues for further analyses.

Patients and tissues samples

The calcific tendon and adjacent normal tendon tissue specimens were obtained from ten clinically confirmed calcific tendinopathy patients who were free from other diseases. The mean age of the calcific tendinopathy patients was 59 years: 5 females, 5 males, ages 44–73 years old. The tendon tissues from calcific tendinopathy patients were collected using an arthroscopic punch, during the removal of arthroscopic calcific deposits and subsequent capsular release of the glenohumeral joint. Using an arthroscopic punch, tissue samples were harvested from calcific tendons during calcium deposit removal in the subacromial space and from subscapularis normal tendons during capsular release of the glenohumeral joint. All patients signed informed consent to use the samples for research, and this study was approved by the Ethics Committee under Southwest Hospital, Army Medical University.

Primary rat tendon cell isolation and culture

Primary rat tendon cells were isolated following the previously described protocols.^{46,47} Achilles tendons were harvested from healthy male SD rats (8-week old) as mentioned above and cut into small pieces of 2–3 mm³. The sliced tissues were placed in 6-well plates, supplemented with Dulbecco's modified Eagle's medium (DMEM) containing 10% fetal bovine serum (FBS) (Gibco) and incubated at 5% CO₂/37°C. Two weeks later, the cells were trypsinized and re-seeded in 100 mm cell culture plates with fresh medium. Medium was changed every three days. Cells between passages 1 and 3 were chosen for experiments.

METHOD DETAILS

Gene expression dataset

The dataset of PPP1R3A expression in nonlesional and lesional tendons from patients with tendinopathy was downloaded from GSM 26051 (<http://www.ncbi.nlm.nih.gov/geo/query/acc.cgi?acc5GSM26051>).²⁰ Expression data were available for 23 samples.

Histology, immunohistochemistry, and immunofluorescence assays

Tissue sections were fixed in 4% paraformaldehyde overnight. The sections were then washed with running water and dehydrated with ethanol. Vitrification was carried out using dimethylbenzene followed by paraffin embedding. For immunohistochemistry, sections were deparaffinized in xylene and subsequently hydrated with ethanol. Following hydration, the sections were stained with hematoxylin and eosin (HE), safranin O, or Masson trichrome. Histology scores were calculated semi-quantitatively based on six parameters: fiber structure, fiber arrangement, inflammation degree, vessel number, cell number, and roundness of cell nuclei. Normal fibroblast-like cells were characterized by an elliptical or spindle-shaped nucleus whereas inflammatory cells were chosen based on round-shaped nucleus. For immunological analyses, paraffinized sections were incubated with a primary antibody against PPP1R3A (anti-PPP1R3A, Absin, 1:100, abs134647), Collagen I (anti-COL I, Abcam, 1:100, Cat# ab270993, RRID:AB_2927551), TNMD (anti-TNMD, Absin, 1:400, abs155667), osteocalcin (anti-OCN, Santa Cruz Biotechnology, 1:50, Cat# sc-390877, RRID:AB_2937079), Sox9 (anti-Sox9, Santa Cruz Biotechnology, 1:50, Cat# sc-166505, RRID:AB_2255399), SERCA2 (anti-SERCA2, 1:50, Santa Cruz Biotechnology, Cat# sc-376235, RRID:AB_10989947) or Piezo1 (anti-Piezo1, 1:50, Proteintech, Cat# 15939-1-AP, RRID:AB_2231460) overnight. The sections were then washed three times with PBS and incubated with a corresponding secondary antibody that was either horse radish peroxidase-conjugated (immunohistochemistry) or fluorescein-conjugated (immunofluorescence) for 1.5 h at room temperature. Images were acquired using confocal microscopy (Nikon A1R, Japan, RRID:SCR_020319).

Reconstruction of plasmids and lentivirus packing

Total RNA was isolated from rat tendon tissue using a TRIzol Plus RNA Purification Kit (Invitrogen, Carlsbad, CA, USA) following the manufacturer's instructions. PPP1R3A fragment was amplified from rat total RNA using primers from Table S1. PPP1R3A coding sequence was cloned into a lentiviral expression vector pCDH-CMV-MCS-EF1-copGFP (System Biosciences, SBI, Palo Alto, CA, USA) through BamHI and NotI sites. EcoRI site and Kozak consensus sequence were added to the forward primer, and BamHI site was added to the reverse primer. The PCR product and lentiviral vector were first digested with EcoRI and BamHI restriction enzymes (New England Bioscience, Ipswich, MA, USA) separately and then ligated together using T4 ligase (Takara, Kusatsu, Japan). The reconstructed plasmid was verified by sanger sequencing. The empty vector served as a negative control. For lentivirus packing, HEK293T cells (ATCC, Cat# CRL-3216, RRID:CVCL_0063) were co-transfected with a control vector or vector carrying PPP1R3A fragment, and lentiviral packaging mix using Lipofectamine 2000 (Invitrogen, Carlsbad, CA, USA). Three days post transfection, the culture medium was collected, filtered through a 0.45- μ m filter, and then incubated with polyethylene glycol 8000 (PEG 8000) for 12 h at 4°C before subjected to concentration at 4000 \times g for 20 min. Concentrated lentivirus was stored at –80°C until further use.

The tendon cells were seeded in 6-well plates (Corning, Corning, NY, USA) at a density of 5×10^5 cells/ml and transduced with either virus of equal titer. Sixteen hours later, the medium was replaced by 2 mL of fresh complete medium. At 72 h after lentiviral transduction, PPP1R3A mRNA and protein expression level in tendon cells were measured by RT-qPCR and Western blot analysis.

siRNA transfection

Small interfering RNAs (siRNAs) targeting rat PPP1R3A, Piezo1 or HuR and non-specific negative control oligos (siControl) were purchased from GenePharma (Shanghai, China). The siRNA targeting sequences were listed in Table S1. Transfection was performed using Lipofectamine 3000 (Invitrogen, Carlsbad, CA, USA) following the manufacturer's protocol. Briefly, cells were seeded at 1×10^5 cells/well in 24 well plates and the transfection complex (containing 1.5 μ L Lipofectamine 3000 and siRNAs) was added directly to the medium. Cells were harvested 48 h post transfection for RNA and protein analyses.

Quantitative real-time PCR

Total RNA was extracted using TRIzol reagent (Invitrogen). First-strand cDNA of the total RNA was synthesized with a PrimeScript RT reagent kit (TaKaRa, Tokyo, Japan). Subsequently, cDNA samples were synthesized and amplified with SYBR Premix Ex Taq II (Takara) and an ABI PRISM 7900 Sequence Detection System (Life Technologies, Grand Island, NY, USA). RT-qPCR analysis was carried out by using the primer pairs from Table S2. GAPDH was used as an endogenous control. Relative expression levels of the genes were calculated using the $2^{-\Delta\Delta CT}$ method.

Western blot analysis

Tendon cells were harvested and washed with PBS. Cells were resuspended in RIPA lysis buffer and incubated for 60 min. The remaining lysate was loaded onto 10% or 15% sodium dodecyl sulfate (SDS) gels and the proteins were separated by polyacrylamide electrophoresis (PAGE). Subsequently, the proteins were transferred onto nitrocellulose membranes, and the membranes were blocked using 5% bovine serum albumin (BSA) in PBS-Tween for 1 h. After blocking, the membranes were incubated with the corresponding primary antibodies (Rabbit anti-PPP1R3A, 1:500, Absin, Abs134647; Mouse anti-GAPDH, 1:1000, Santa Cruz Biotechnology, Cat# sc-365062, RRID:AB_10847862; Mouse anti-OCN, 1:500, Santa Cruz Biotechnology, Cat# sc-390877, RRID:AB_2937079; Mouse anti-Sox9, 1:500, Santa Cruz Biotechnology, Cat# sc-166505, RRID:AB_2255399; Mouse anti-SERCA2, 1:500, Santa Cruz Biotechnology, Cat# sc-376235, RRID:AB_10989947; Rabbit anti-Piezo1, 1:200, Proteintech, Cat# 15939-1-AP, RRID:AB_2231460; Rabbit anti-HuR, 1:1000, Abcam, Cat# ab200342, RRID:AB_2784506; Mouse anti- α -Tubulin, 1:200, Santa Cruz Biotechnology, Cat# sc-8035, RRID:AB_628408) overnight at 4°C. The next day, the membranes were washed three times in PBS-T and incubated with goat anti-rabbit (Beyotime, 1:1000, Cat# A0208, RRID:AB_2892644) or goat anti-mouse HRP-conjugated secondary antibody (Beyotime, 1:2000, Cat# A0216, RRID:AB_2860575) for 1 h at room temperature. The membranes were once again washed three times with PBS-T and visualized using chemiluminescence.

Cell proliferation assay

Proliferation of cells *in vitro* was quantified using CCK8 commercial kit from Beyotime (Shanghai, China, C0038) according to manufacturer's protocol. Briefly, cells from different time points (hour 12, 24, 48, 72 and 96) were incubated in 10% CCK-8 solution at 37°C for 1 h. The supernatant develops a brown color (formazan derivative formed by cell metabolism) and the intensity directly correlates with cell proliferation. The optical density of the supernatant was measured at 450 nm using a microplate reader SpectraMax 190, Molecular Devices, RRID:SCR_018932).

Cell osteogenic differentiation induction

Osteogenic differentiation was induced in tendon cells by incubation with osteogenic medium (DMEM high containing 100 nmol/L dexamethasone, 0.2 mmol/L of ascorbic acid, 20 mmol/L β -glycerol phosphate, 10% FBS). Successful differentiation was verified using alkaline phosphatase activity and alizarin red staining.

Alkaline phosphatase activity and alizarin red-S staining

Alkaline phosphatase (ALP) activity was evaluated using the BCIP/NBT color kit (Nanjing Jiancheng Bioengineering Institute, Nanjing, China, I023-1-1) according to manufacturer's instructions. The concentration of ALP was determined using ALP assay kit (Beyotime, P0321S) and the total protein was estimated using BCA kit (Pierce, ThermoFisher, Rockford, IL, USA) according to manufacturer's protocol. ALP activity was determined relative to that of the control and all samples were normalized to the total protein content.

For alizarin red-S staining, cells were fixed with 95% ethanol and stained in 1% ARS staining solution (pH 4.2; Sigma-Aldrich, TMS-008) for 20 min at room temperature. 100-mmol/L cetylpyridinium chloride (Sigma-Aldrich, C0732-100G) was added to the solution and incubated for 1 h. The optical density of the solution was measured at 562 nm with an EnSpire multimode plate reader (PerkinElmer, Waltham, MA). Relative ARS intensity was calculated relative to that of the control.

Cytosolic Ca²⁺ measurement

Cells were seeded in 6-well plates coated with poly-D-lysine and incubated with 5 μ M Fura-4/AM (Beyotime, S1060) dissolved in Hank's balanced salt solution (HBSS). Pluronic F 127 (Beyotime, ST501-0.1g) was added to a final concentration of 0.05% and incubated for 30 min. Imaging was performed using a Zeiss LSM 510 META confocal microscope (Carl Zeiss AG, RRID:SCR_018062).

Calcium ion detection

To detect intracellular Ca²⁺ ions, cells were incubated for 1 h with 10 μmol Fura-4/AM under gentle oscillation. Free dye was washed by rinsing the cells with calcium-free buffer. The cells were analyzed by flow cytometry and the fluorescence intensity was recorded as the F value. For calculation of F_{max}, cells were permeabilized with 1% Triton X-100 for 30 min at room temperature, incubated with CaCl₂ for 10 min prior to measuring the intensity by flow cytometry. For F_{min} calculation, 10 mM EDTA was used as a chelating agent for 10 min prior to measuring the fluorescence at 488 nm. Total calcium ion concentration was calculated as follows: $[Ca^{2+}]_{free} = K_d [F - F_{min}] / [F_{max} - F]$, $K_d = 390$ Nm.

RNA immunoprecipitation (RIP) analysis

To assess the association of endogenous HuR with endogenous PPP1R3A mRNA, RIP assay was performed using a Magna RIP RNA Binding Protein immunoprecipitation Kit (Millipore, Bedford, MA, USA, 17–700) according to the manufacturer's instructions. Briefly, tendon cells (2×10^7) were collected, and lysates were used for IP overnight at 4°C in the presence of excess (30 μg) IP antibody (IgG, anti-HuR). The next day, magnetic beads were added to the samples and incubated for 1 h. Subsequently, Proteinase K was added and incubated at 55°C for another hour. RNA was isolated using an RNA extraction reagent (Solarbio, Beijing, China) and the mRNA levels of PPP1R3A and GAPDH were detected by qRT-PCR analysis.

Biotin pull-down assays

Biotinylated transcripts were generated from PCR-amplified DNA fragments using T7 RNA polymerase in the presence of biotin-UTP. All sequences of oligonucleotides for synthesizing full-length PPP1R3A 5'-UTR, CR, or 3'-UTR are described in Table S1. One microgram of purified biotinylated transcripts was incubated with 30 μg of cell lysates for 30 min at room temperature. RNA-bound complexes were isolated using paramagnetic streptavidin-conjugated Dynabeads (Invitrogen), and the pull-down fraction was analyzed by Western blot.

Luciferase reporter assay

To construct pGL3-derived reporter vectors, the 5'-UTR, CR, and 3'-UTR fragments of PPP1R3A mRNA were amplified by PCR. All primer sequences for generating these constructs are provided in Table S4. The 5'-UTR, CR, and 3'-UTR fragments of PPP1R3A were inserted between the NheI and XhoI sites of pGL3-promoter vector (Promega, WI, USA, E1761). Luciferase reporter assay was performed following the described previously protocol.⁴⁸ Briefly, cells were seeded in 24-well plates (1×10^5 cells per well) and transfected with siRNA targeting HuR. Twenty-four hours post transfection, cells were transfected again with the pGL3-derived reporters together with a pRL-CMV vector (Promega, E2261) and cultured for 48 h. Firefly and renilla luciferase activities were measured with a double luciferase assay system (Promega, E1910) following the manufacturers' protocol. Firefly luciferase measurements were normalized to renilla luciferase measurements from the same sample.

RNA half-life analysis

RNA half-life at different time points were evaluated by adding actinomycin D (final concentration 2 μg/mL, Sigma-Aldrich) to the cell culture medium 48 h post siRNA treatment. Total RNA was extracted at 0, 1, 2, 3, and 4 h after actinomycin D treatment and mRNA levels were analyzed by qPCR.

QUANTIFICATION AND STATISTICAL ANALYSIS

All experiments were performed as at least three independent repeats unless mentioned otherwise and presented as means ± SD. Comparisons between two groups were assessed by using Mann-Whitney U test and two-tailed Student's t tests using GraphPad Prism 5 software (GraphPad Software, La Jolla, CA, USA, RRID:SCR_002798). A value of $p < 0.05$ (*, #) or $p < 0.01$ (**, ##) were considered as statistically significant. All of the statistical details of experiments can be found in the figure legends.